NAVAL POSTGRADUATE SCHOOL

MONTEREY, CALIFORNIA

THESIS

MODELING OF A MICRO-ELECTRONIC-MECHANICAL SYSTEMS (MEMS) DEFORMABLE MIRROR FOR SIMULATION AND CHARACTERIZATION

by

Mark C. Mueller

September 2016

Thesis Advisor: Fabio Alves
Co-Advisor: Andres Larraza

THIS PAGE INTENTIONALLY LEFT BLANK

REPORT DOCUMENTATION PAGE			*Form Approved OMB No. 0704-0188*

1. AGENCY USE ONLY *(Leave blank)*	**2. REPORT DATE** September 2016	**3. REPORT TYPE AND DATES COVERED** Master's thesis

4. TITLE AND SUBTITLE MODELING OF A MICRO-ELECTRONIC-MECHANICAL SYSTEMS (MEMS) DEFORMABLE MIRROR FOR SIMULATION AND CHARACTERIZATION	**5. FUNDING NUMBERS**
6. AUTHOR(S) Mark C. Mueller	
7. PERFORMING ORGANIZATION NAME(S) AND ADDRESS(ES) Naval Postgraduate School Monterey, CA 93943-5000	**8. PERFORMING ORGANIZATION REPORT NUMBER**
9. SPONSORING /MONITORING AGENCY NAME(S) AND ADDRESS(ES)	**10. SPONSORING / MONITORING AGENCY REPORT NUMBER**

11. SUPPLEMENTARY NOTES The views expressed in this thesis are those of the author and do not reflect the official policy or position of the Department of Defense or the U.S. Government. IRB Protocol number ____N/A____.

12a. DISTRIBUTION / AVAILABILITY STATEMENT Approved for public release. Distribution is unlimited.	**12b. DISTRIBUTION CODE**

13. ABSTRACT (maximum 200 words)

Development of a model that can simulate the wavefront-altering effects of a micro-electro-mechanical system (MEMS) mirror has many potential research benefits. Without the need to purchase costly lab equipment and/or wait for mirror fabrication, the use of model simulation would allow users to optimize various parameters of a device before fabrication.

Research focused on developing models for two of the most common types of MEMS mirrors: segmented and continuous face sheet devices. Models for these devices were first constructed in MATLAB and then experimentally verified in order to characterize and compare the differences in behavior between model and measured results.

The models developed displayed similar results when compared to interferometric readings taken from an actual MEMS mirror. The models were able to reduce the wavefront error of a notional distorted wave. The corrected wavefront of the notional wave compared well with experimental data collected indicating that the models were good representations compared to actual devices of their specific type.

14. SUBJECT TERMS Adaptive optics, deformable mirror, MEMS	**15. NUMBER OF PAGES** 55
	16. PRICE CODE

17. SECURITY CLASSIFICATION OF REPORT	**18. SECURITY CLASSIFICATION OF THIS PAGE**	**19. SECURITY CLASSIFICATION OF ABSTRACT**	**20. LIMITATION OF ABSTRACT**
Unclassified	Unclassified	Unclassified	UU

NSN 7540-01-280-5500 Standard Form 298 (Rev. 2-89) Prescribed by ANSI Std. 239-18

THIS PAGE INTENTIONALLY LEFT BLANK

Approved for public release. Distribution is unlimited.

MODELING OF A MICRO-ELECTRONIC-MECHANICAL SYSTEMS (MEMS) DEFORMABLE MIRROR FOR SIMULATION AND CHARACTERIZATION

Mark C. Mueller
Lieutenant, United States Navy
B.S., United States Naval Academy, 2010

Submitted in partial fulfillment of the
requirements for the degree of

MASTER OF SCIENCE IN APPLIED PHYSICS

from the

NAVAL POSTGRADUATE SCHOOL
September 2016

Approved by: Fabio Alves
Thesis Advisor

Andres Larraza
Co-Advisor

Kevin Smith
Chair, Department of Physics

THIS PAGE INTENTIONALLY LEFT BLANK

ABSTRACT

Development of a model that can simulate the wavefront-altering effects of a micro-electro-mechanical system (MEMS) mirror has many potential research benefits. Without the need to purchase costly lab equipment and/or wait for mirror fabrication, the use of model simulation would allow users to optimize various parameters of a device before fabrication.

Research focused on developing models for two of the most common types of MEMS mirrors: segmented and continuous face sheet devices. Models for these devices were first constructed in MATLAB and then experimentally verified in order to characterize and compare the differences in behavior between model and measured results.

The models developed displayed similar results when compared to interferometric readings taken from an actual MEMS mirror. The models were able to reduce the wavefront error of a notional distorted wave. The corrected wavefront of the notional wave compared well with experimental data collected indicating that the models were good representations compared to actual devices of their specific type.

THIS PAGE INTENTIONALLY LEFT BLANK

TABLE OF CONTENTS

THIS PAGE INTENTIONALLY LEFT BLANK

LIST OF FIGURES

THIS PAGE INTENTIONALLY LEFT BLANK

LIST OF TABLES

THIS PAGE INTENTIONALLY LEFT BLANK

I. INTRODUCTION

Micro-electronic-mechanical systems (MEMS) encompass a variety of devices at the micro and nano level. Devices that operate at such a scale offer a number of advantages in addition to size, such as reduced power consumption, a reduction in material required, and are suitable for large batch manufacturing. Examples of systems in which these mechanisms can be used include springs, cantilevers, sensors, mirrors, switches, and motors.

A. BACKGROUND

MEMS devices are usually fabricated in large lots on silicon wafers, but glass, ceramics, metals, and plastics can be used. These devices are manufactured with a variety of techniques, including bulk micromachining, which etches the surface of the material; surface micromachining, which puts down subsequent layers on top of the surface; or a combination of these techniques. The basic manufacturing process starts with the deposition of materials onto the substrate wafer. Once deposited, the material is patterned in order to sketch the outline of the desired shape. The wafer is then etched to remove unwanted material. This process is repeated using a multitude of different methods for deposition, patterning, and etching until the desired design of the device is achieved.

While a large number of devices can be created efficiently at a relatively low cost, the creation of a single device is much more cost prohibitive. A main concern regarding collective batch manufacturing is that it limits the device being constructed to the specific sequence, method, and materials for that production run. Additionally, manufacturing via micromachining is not perfect. Often multiple copies of the same design have to be created to achieve a single functioning device.

B. PURPOSE

Manufacturing large optics for use in space requires large, heavy, and expensive materials. An array of micro mirrors that adjust their height in order to deform their surface enables lighter and less-expensive materials to replace traditional large optics.

Lighter materials do not have the same high optical qualities, but the array of mirrors could correct for the wavefront aberrations by deforming on command. The goal of this thesis is to develop and validate two types of MEMS mirror models for predicting enhancements to wavefront correction.

II. MODEL DESIGN

MEMS deformable mirrors are ideal for wavefront correction due to their high actuator density, relative low cost, small size, and low power consumption. These devices have demonstrated repeatability in actuator piston position movement accuracy [1]. Other types of deformable mirrors, such as pizo-electric devices, cost more, have higher power requirements, and possess a significant logistics tail tied to cabling and server support for the device.

MEMS mirrors are deformed using electrostatic actuators that are normal to the surface and located below an electrostatically actuated diaphragm supported along two edges above a fixed electrode. The mirror surface is connected to the top surface of the actuator by an electrostatically actuated diaphragm, as shown in Figure 1. Typically, the layers are made of polysilicon with a thin, reflective film applied to the top layer to form the mirror.

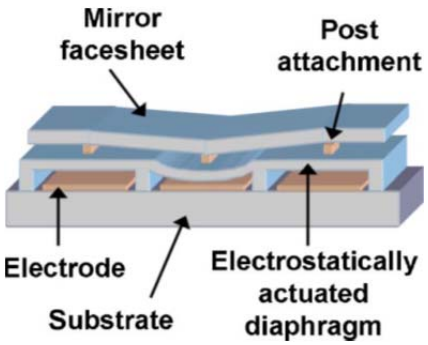

According to Steward et al. [2], this diagram depicts a row of thee actuators on a continuous face sheet MEMS DM in which the middle actuator has a voltage applied causing the surface face sheet to be pulled down at that location.

Figure 1. Continuous Face Sheet MEMS DM. Source: [2].

There are three primary types of MEMS mirrors: continuous face sheet, segmented, and tip and tilt. A continuous face sheet mirror is a surface that has a continuous membrane along the entire length of the surface. This produces a coupled mechanical system. A segmented mirror is made of tightly packed mirror segments. The empty space between mirrors is called the fill factor. Segmented mirrors can come in a

variety of shapes from square to hexagonal. For this research, a segmented mirror is defined as a device that only has vertical motion. A tip and tilt mirror allows each segment to move vertically and tilt along a 360 degree arc around the piston. Figure 2 is a depiction of both types of actuation.

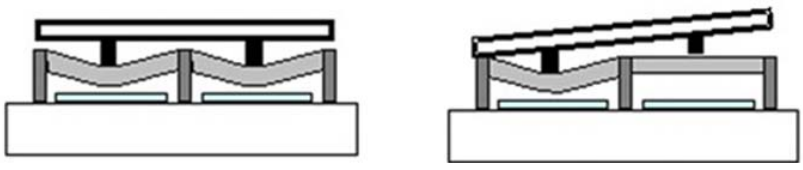

As demonstrated by Stewart et al. [3], a single actuator from a segmented DM is shown being stimulated in piston only movement (a) and with tip-tilt (b). Even though a single DM mirror segment is shown, two actuators are visible and are required to have their diaphragms actuated with different voltages in order to create the tilt as presented. If tip and tilt are not desired then a single mirror segment can be attached to one actuator. [3]

Figure 2. Piston (a) and Tip-Tilt (b) DM. Source: [3].

A. ACTUATOR MODEL

The continuous face sheet MEMS mirror was considered for this research, as it is the most complex mirror type. This device is composed of two mechanical systems: an array of actuations and a non-linear continuous face sheet. The two systems are coupled.

The continuous face sheet model achieves deformation by applying a force on an actuator. This force causes the sheet to displace at both the actuator location and at unactuated neighbors coupled near the active segment, as shown in Figure 3.

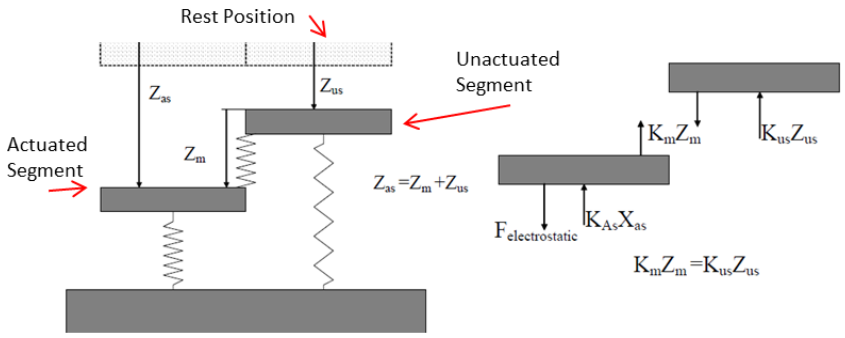

From to Papvasiliou et al. [4], this is a depiction of the coupled system for a continuous face sheet MEMS in relation to how unactuated segments are influenced by their actuated neighbor. The actuated segment, Z_{as}, is pulled down from its rest position to its unactuated spot, Z_{us}, due to the coupling by Z_m. The associated free body diagram is shown to the right of the image.

Figure 3. Coupled Actuated Effects on Adjacent Unactuated Segments. Adapted from [4].

When a voltage difference is applied between plates, an opposite charged electrostatic force develops and pulls the plate down. This decreases the mirror's height since the plate is connected to the mirror surface through a post attachment. The surface of a continuous face sheet mirror is smooth, which creates a curved displacement on its surface (as seen in Figure 4).

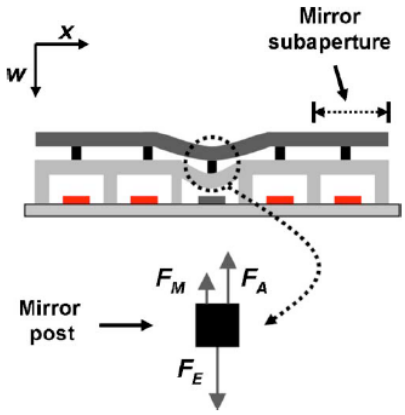

According to Steward et al. [2], the curved appearance on the surface of a continuous face sheet DM being deformed due to a single actuator. The electro static force F_E pulls down the surface and is the same as Z_{as} while the force of the membrane F_M corresponds to Z_m and the restoring force, F_A to Z_{us} as was shown in Figure 3.

Figure 4. Free Body Diagram of an Actuated Pixel. Source: [2].

The electrostatic force pulling on the membrane is modeled as

$$F_E = \frac{\varepsilon A V^2}{2(g-w)^2}, \tag{3.1}$$

where ε is the permittivity of the media, A is the area of the plate, g is the separation between plates, V is the applied voltage, and w is the displacement of the plate. The restoring force, F_A, is a result of the opposing force and modeled through Hooke's law. The spring constant is represented by k and w is the deflection.

$$F_A = -kw \tag{3.2}$$

The electrostatic force and opposing force are both local to the actuator, while the mirror force, F_M, is coupled to the rest of the system and is the sum of these two local forces.

B. SURFACE MEMBRANE MIRROR MODEL

Figure 5 shows a cross section of Figure 6 with the key physical elements labeled.

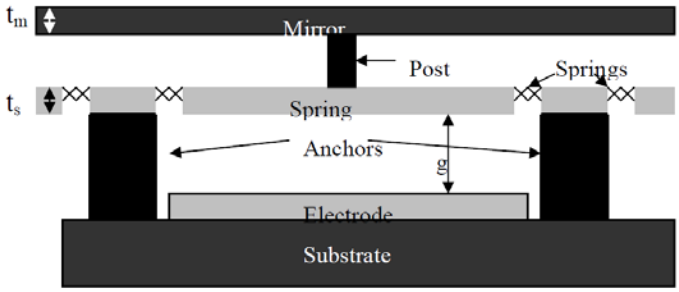

From Azucena et al. [5], a cross-sectional view of a MEMS DM showing the labeling of all relevant physical elements. The thickness of the mirror is represented by t_m, the electrostatically actuated diaphragm, is t_s. The distance between plates, g is also known as the gap and the region encompassing the gap is referred to as the diaphragm.

Figure 5. Cross-Sectional View of a MEMS DM. Source: [5].

When deformations are smaller than the thickness of the mirror face sheet the surface can be modeled by using the plate equation:

$$\nabla^4 w(x,y) = \frac{q(x,y)}{D}, \tag{3.3}$$

where $q(x,y)$ is the load distributed normally in N/m^2 on the surface and $w(x,y)$ is the desired mirror shape. *D* is the flexural rigidity of the plate in which *D* is given by:

$$D = \frac{Eh^3}{12(1-v^2)}, \tag{3.4}$$

where the thickness of the face sheet is *h*, *v* is Poisson's ratio and *E* is Young's modulus. If the mirror is deflected more than the thickness of the face sheet, the mirror's surface is stretched due to plain strain on the surface. In order to account for the mechanical coupling of actuators the plate equation must be modified to [6]:

$$\nabla^4 w(x,y) = \frac{q(x,y)}{D} + \frac{6}{h^2}\left\{\left[\left(\frac{\partial w(x,y)}{\partial x}\right)^2 \frac{\partial^2 w(x,y)}{\partial x^2}\right] + \left[\left(\frac{\partial w(x,y)}{\partial y}\right)^2 \frac{\partial^2 w(x,y)}{\partial y^2}\right]\right\}. \tag{3.5}$$

Equation (3.5) can be adapted into an algebraic expression in order to solve for the plate displacement $w(x,y)$ by means of Navier's method for a linear system. In this method, the following boundary conditions can be applied for a rectangular plate [7],

$$(w)_{x=0,x=a} = 0 \quad (w)_{y=0,y=b} = 0$$

$$(m)_{x=0,x=a} = 0 \quad (m)_{y=0,y=b} = 0,$$

where *m* and *n* represent index locations. Applying the above boundary conditions results in the algebraic expression for the deflection:

$$w(x,y) = \sum_{m=1}^{M}\sum_{n=1}^{N} W_{mn} \sin\frac{m\pi x}{a} \sin\frac{n\pi y}{b}, \tag{3.6}$$

where *M* and *N* represent new index locations and give the dimensions of the matrix for the number of actuators in each row and column. The values *a* and *b* are the length and width of the mirror, respectively. Since deflection theory for plates is not always linear, a more robust method is required to solve for the initial value of *W*. Galerkin's method is one such solution that can be applied. It transforms a large set of problems by converting a given set of differential equations into definite integrals:

$$\iint [D\nabla^2\nabla^2 w(x,y) - q(x,y)] \sin\frac{m\pi x}{a} \sin\frac{n\pi x}{b}\, dxdy = 0. \tag{3.7}$$

The plate equation can be expressed in matrix form and reduced such that W can be solved iteratively by estimating initial deflection and then solving for W until convergence is achieved. The value of W can then be placed into the algebraic equation to solve for the deflection,

$$\left[\left(\left(\frac{m}{a}\right)^2+\left(\frac{n}{b}\right)^2\right)^2\right]W=\frac{4}{Dab\pi^4}\sum_{c=1}^{R}\left(-kw_c+\frac{\varepsilon A}{2(g-w_c)^2}\right)V_c^2 sin\frac{m\pi x}{a}sin\frac{n\pi y}{b}, \quad (3.8)$$

where V_c is voltage applied at each actuator, represented by c in the x and y direction. R represents the number of actuators.

When the actuators are expressed in a symmetrical square pattern, the influence matrix can be modeled as a cubic form [8]. As this form is a less computationally intensive method than previously discussed approaches, the following Gaussian influence function generates the displacement of the mirror surface,

$$W(x,y)=\frac{2\pi}{\lambda}\exp\left\{\frac{lnb\left[(x-x_c)^2+(y-y_c)^2\right]}{d^2}\right\}, \quad (3.9)$$

where b is the Gaussian index and d is the distance between adjacent actuators [9]. The surface's shape is modeled by applying the appropriate voltage at the specified location.

$$w(x,y)=\sum_{c=1}^{R}V_c W_c(x,y) \quad (3.10)$$

A continuous face sheet DM offers benefits over a segmented mirror, as there is no gap on the continuous sheet's surface mirror that would result in photons being lost. Additionally, the smooth surface can be used for phase modulation, and light striking an edged surface introduces diffraction effects. The MATLAB code that generates the continuous and segmented models is included in the Appendix.

C. MEMS SEGMENT MIRROR MODEL

The mirrors in a segmented mirror are not physically coupled, which prevents an actuator from influencing a mirror's neighbors. This simplifies the model to one in which the up and down position of the mirror is directly related to its electrostatic force (F_E) without coupling. However, an artificial coupling between segments can sometimes be desired in order to prevent shading neighboring segments. Artificial coupling also minimizes the effects of diffraction. Detecting a phase difference greater than 2π is difficult using an interferometer. This can result in erroneous data readout. Therefore, a spacing difference in height between adjacent actuators should not exceed one wavelength. Computation times and latency in system response were reduced without surface coupling of the face sheet [10]. The gap between mirror segments is known as the fill factor, which negatively affects the amount of light reflecting off the surface of the DM. This system can also be modeled by a Gaussian function as follows,

$$w(x,y) = \sum_{c=1}^{R} V_c 2\pi e^{\log(gi)\frac{x^2+y^2}{a/R^2}}, \tag{3.11}$$

where *gi* is the Gaussian index.

D. MEMBRANE MODEL VERIFICATION AND VALIDATION

The computational and system latency benefits and validated experiment results drive the decision to use the Gaussian function to model the continuous face sheet. Hudgin et al. [11] investigated error variance for an actively deformed mirror compared to atmospheric turbulence and plotted the resulting data using different functions, as shown in Figure 6.

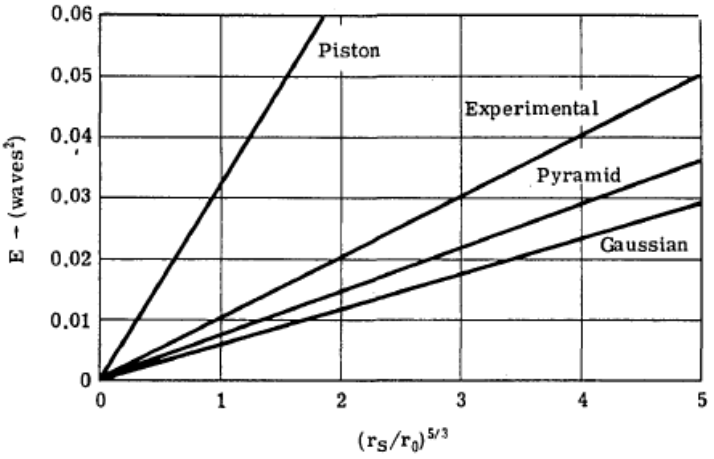

Results from Richard Hudgin et al. [11] for active mirror error variance for atmospheric turbulence showing the fitting error. *rs/ro* is the activator spacing divided by the coherence length for the turbulence. E is the average error variance, but is given in relation to waves, unfortunately the author does not specify the wavelength used.

Figure 6. Active Mirror Error Variance for Atmospheric Turbulence. Source: [11].

While the Gaussian response function is not a perfect match to the experimental data, it is fairly close. Additional experiments by Tyson et al. [12] compared the shape of a mirrors surface in relation to the function used, as shown in Figure 7.

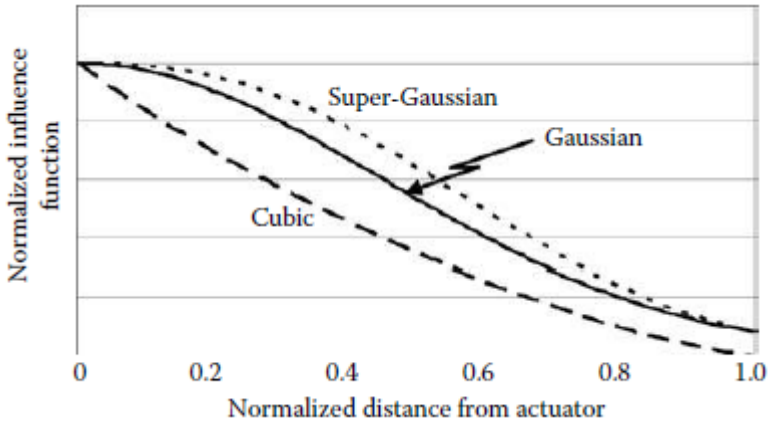

Tyson's graph [12] shows the shape of the deformable mirror after being actuated, where 1.0 represents the location of the actuated piston being fully pulled down. The lines correspond to the respective heights for each modeling shape as distance increase from the pulled down actuator.

Figure 7. Comparison of Membrane DM Shapes. Source: [12].

In Tyson's graph, shown in Figure 7, the shape of the deformable mirror after actuation is referenced as the influence function on the y-axis. This is the standard convention and the shape of the mirror surface is referenced as the influence function for the rest of the paper.

Bifano et al. [13] took surface map measurements using an interferometer for a 10 by 10 continuous face sheet MEMS DM. Using the equations described previously, a 10 by 10 DM model was simulated to compare the model's results with the actual measurements of [13], as shown in Figure 8 (a). The darker surface color represents a downward direction. Results from the simulated model are shown in Figure 8(b).

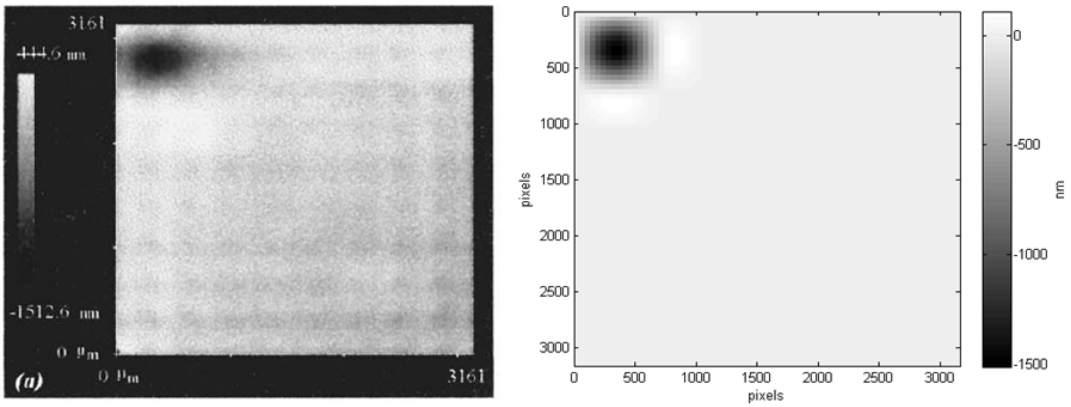

(a) (b)

The article by Bifano et al. [13] does not indicate which actuator was actuated for the reading. From their measurement in the continuous surface map (a), it appears that the actuator is in the second row of the second column (2,2). Using this same location for actuation, a surface map for the continuous DM model was constructed (b) for comparison to actual surface measurements.

Figure 8. Comparison of Experimental and Model Results for a Continuous DM. Source: [13].

The results from the model in Figure 8 (b) are in agreement with the actual measurements shown in Figure 8 (a). The effects of a single actuator influencing its neighbors is seen in the interferometric surface map as the darker, slightly fuzzy halo around the actuated position. This same feature also appears in the model results in Figure 8 (b). In both cases, the dark spot extends to the edge of the DM despite that the

actuated piston is in the second column. This continuation of the DM beyond its localized position indicates that other actuators in the vicinity are also influenced.

E. SEGMENT MODEL VERIFICATION AND VALIDATION

Bifano et al. [13] also took surface map measurements for a 10 by 10 segmented DM with piston-only motion. The segmented mirror model was used to create a 10 by 10 DM in which the actuator in the fifth row of the six columns was actuated. The model results seen in Figure 9 (b) were compared with the surface map measurement taken by Bifano et al. in Figure 9 (a).

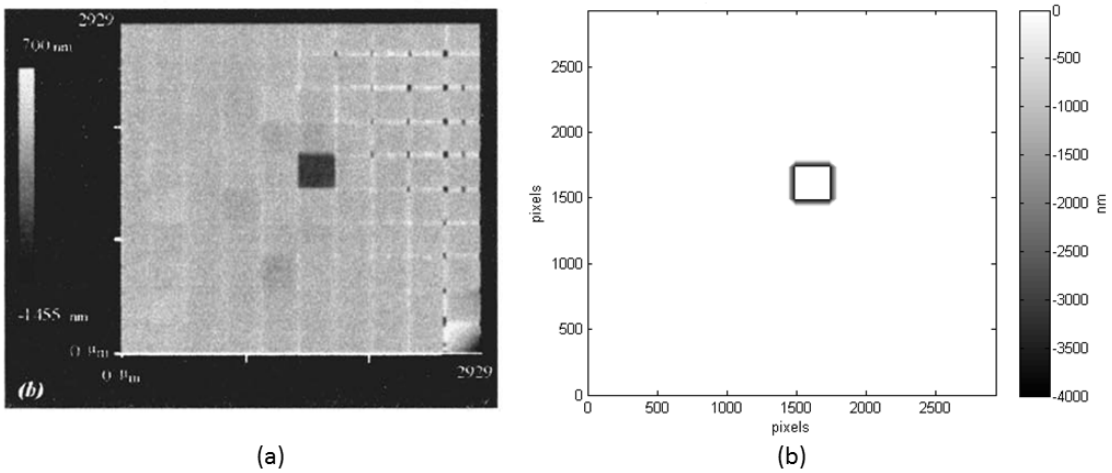

(a) (b)

As explained in Bifano et al. [13], surface map measurements for segmented MEMS DM mirror (a) in comparison to the simulated model results (b) for a 10 by 10 matrix. Measurement in the segmented surface map (a) seems to indicate that the actuator in the fifth row of the sixth column was used. Using this same location for actuation, a surface map for the model (b) was developed for comparison.

Figure 9. Comparison of Experimental and Model Results for a Segmented DM.Source: [13].

Model results shown in Figure 9 (b) are in good agreement with the measurements shown in Figure 9 (a) for the actuated segment. However, the gaps between segments are quite noticeable in Figure 9 (a) as lightly white horizontal and vertical bars. These bars are not present in the simulation results and represent the area where light strikes the DM and is lost. The loss of light ultimately affects the number of photos reaching the focal plane array or science instrument.

III. EXPERIMENTAL SETUP

A. BACKGROUND

For this study, a segmented Boston Micromachines 492 actuator DM was available for experimental lab studies. The goal of the experiment was to characterize the self-correction wavefront performance of the Boston DM. This data was then compared with a simulated wavefront in which the previously constructed DM models. The optical layout for the characterization of the Boston DM is shown in Figure 10.

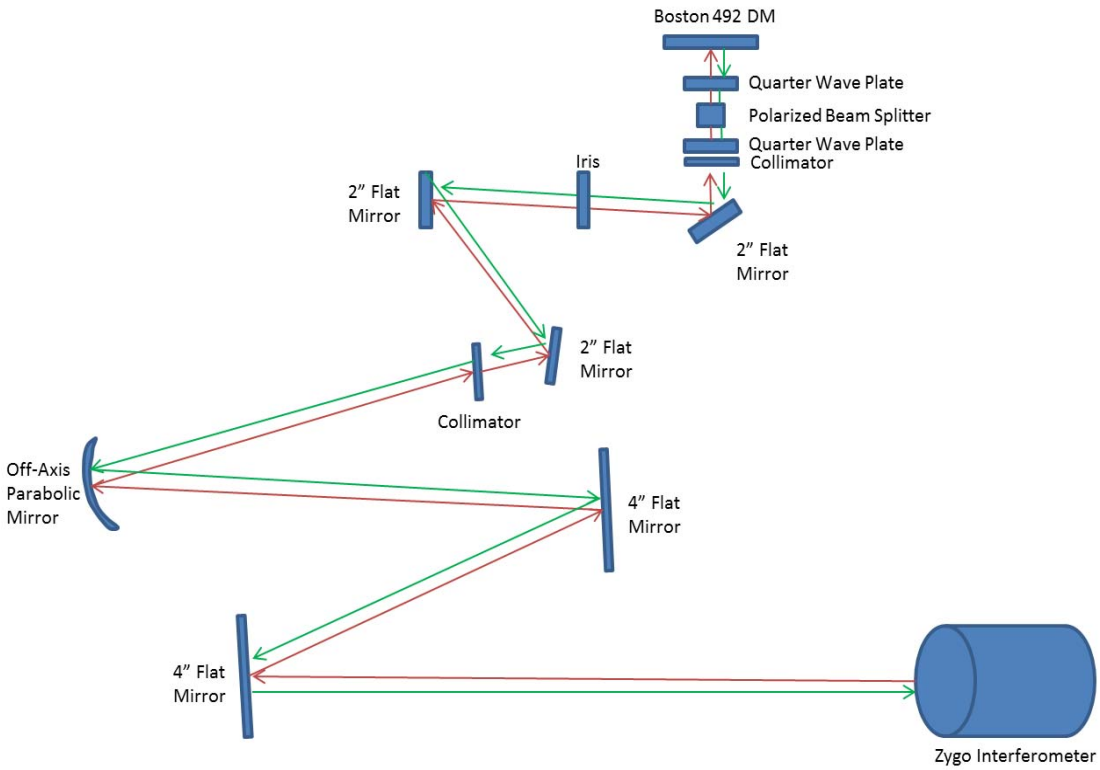

Experimental optical layout for the initial characterization of the Boston 492 DM. The red ray depicts the path of the light from the Zygo interferometer to the DM while the green light shows the path back from the DM to the interferometer.

Figure 10. Experimental Optical Layout for the Boston DM Characterization

Light emanates from the Zygo interferometer in the lower right corner of Figure 10 and is reflected by a series of 4″ flat mirrors until reaching the off-axis parabolic mirror that focuses the light to a 2″ column after passing through a collimator. The light

continues through another series of 2″ flat mirrors before continuing to an iris, forming a circular aperture. For characterization of the DM, light was not polarized so that the rays could pass through both quarter wave plates and the polarized beam splitter without being affected. These plates and beam splitter were part of the layout because the system in Figure 10 is part of a much larger set up that was not involved in this research study.

B. DEFORMABLE MIRROR

A Boston Micromachines 492-SLM deformable mirror consisting of a segmented polysilicon surface wired bonded to a ceramic chip and housed inside a sealed enclosure was used. The system provides fast control and high voltage response up to 205V resulting in a maximum stroke of 1.8μm. Although the mirror has 492 actuators, only 391 of them are visible due to the aperture of the interferometer. The device has a time response of < 20 μsec and an aperture size of 6.9 mm.

While the mirror has the capability to deflect up to 205 volts, it was observed that nonlinearities appeared on the surface of the actuated segments when higher voltages were applied. These irregularities are due to the intrinsic internal stresses on the mirror. Due to these stresses, the mirror surface will not be perfectly flat either when actuated or relaxed, and it will appear slightly domed shaped as shown in Figure 11.

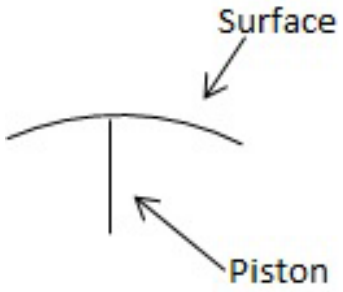

The curved surface for each mirror segment of the DM is a result of intrinsic internal stresses on the individual mirrors regardless of being actuated or in a relaxed state.

Figure 11. Side View Showing the Curved Surface on a DM Segment

Initially, a voltage of 100V was applied to all the actuators in order to achieve a known, biased flat that could be used as a reference. Pulling all the actuators to an initial

starting point allows for segments either to be pushed up above the floor by decreasing the voltage or to be pulled down by increasing the voltage. Another 100V was applied one actuator at a time in order to build the influence matrix. This resulted in each actuator receiving 200V. This voltage, as shown in Figure 12, caused the actuator surface to appear sloped instead of domed-shaped.

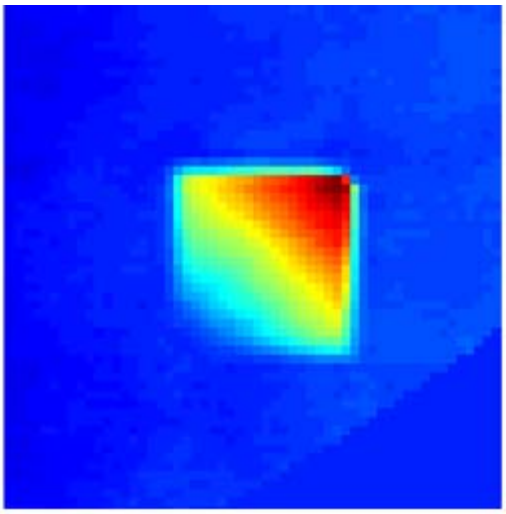

Boston 492-DM single actuator deflection with 100V applied. The surface colors represent the relative height of a pixel in relation to one another. Dark red is a high spot while blue indicates a lower value. The image shows that the segmented surface appears to be slanted which is a result of nonlinearities in the system. Since the surrounding area around the segment is blue, a low spot, this indicates that the segment is being poked.

Figure 12. Boston 492-DM Single Actuator Deflection with 100V Applied

The initial reference voltage was reduced to 50V with the corresponding actuator activation occurring at 100V resulting in the expected dome shape seen in Figure 13.

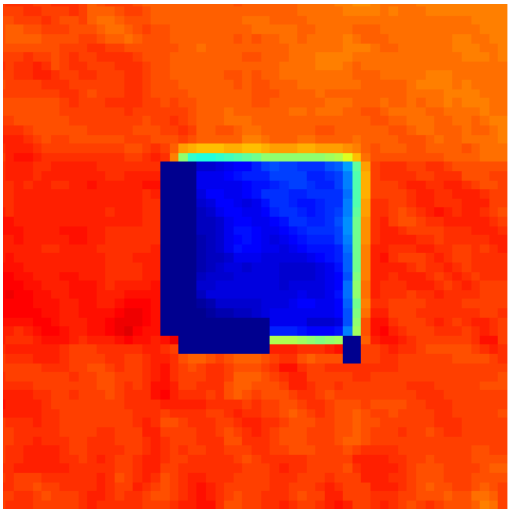

Boston 492-DM single actuator deflection with 50V applied. The surface colors represent the relative height of a pixel in relation to one another. Dark red is a high spot while blue indicates a lower value. The image shows that the segmented surface appears to be correctly pulled down as denoted by the dark blue square with a slight dome shape as seen by the rainbow of colors inscribing the blue square from its higher surrounding of red.

Figure 13. Boston 492-DM Single Actuator Deflection with 50V Applied

Of the 391 actuators visible in the circular interferometer aperture, actuators 1, 43, and 61 would not operate. When activated, a MEMs DM pulls the surface of the mirror down. This is easily seen in Figure 13 in which the actuator is lower than its surroundings, indicated in blue. In Figure 12, the actuator is red while its surroundings are blue, which indicates that the actuator is higher than its surroundings. This poke effect seen is a result of all the initial actuators pulled down to the biased flat except the malfunctioning actuator. As the actuator sticks out from its surroundings even though the same voltage is being applied to all the actuators, it is likely that the actuator did not pull down even though voltage was being applied. The poke effect also appeared when the segmented actuator distance was greater than 2π as compared to the wavelength of the interferometer.

C. WAVEFRONT SENSOR

A Zygo GPI XPHR laser interferometer was used to sense the wave front error and pass the data to a workstation running MetroPro software. The interferometer used at NPS is shown in Figure 14.

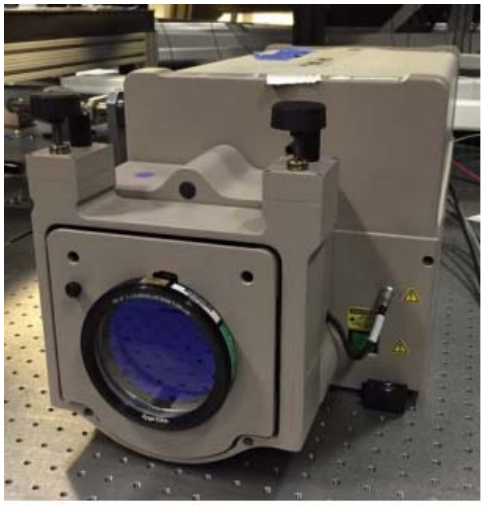

As stated in Villalba [14], the Zygo GPI XPHR Laser Interferometer used is a high resolution, high speed camera that uses optical phase shifting interferometry to measure the wavefront from the DM and 1-meter CFRP mirror. A 632.8nm beam of light was used for conducting measurements.

Figure 14. Zygo GPI XPHR Laser Interferometer at NPS. Source: [14].

The MetroPro software analyzes the data from the interferometer and depicts the wave front on the support computer. The software also corrects for some aberrations such as power, astigmatism, and tilt. A sample output of the software is depicted in Figure 15.

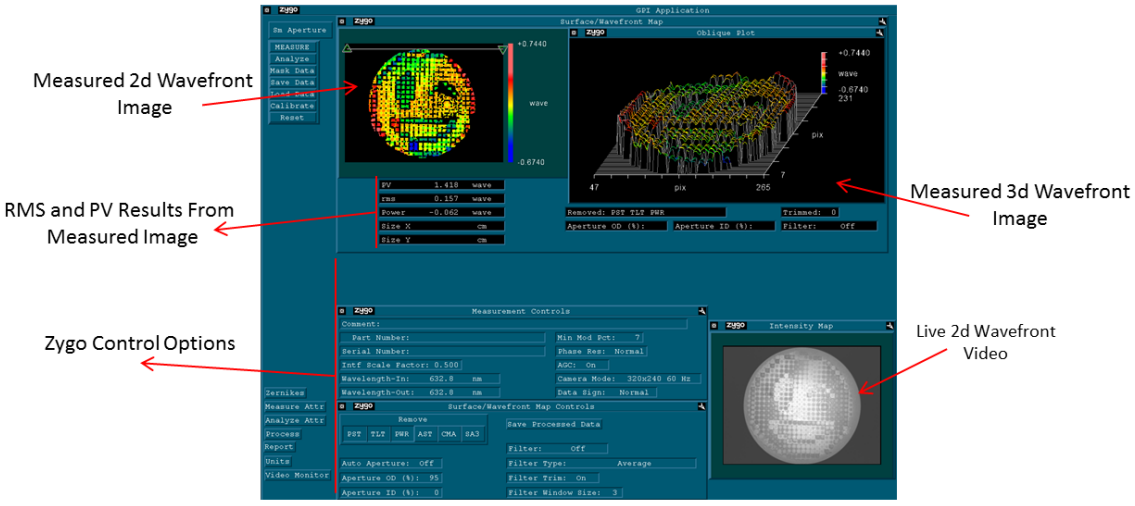

Adaptation of a screenshot from the MetroPro software user interface indicating the control options, measured results, and live stream of data.

Figure 15. MetroPro Software Screenshot

The root mean square (RMS) value is a key parameter in the measurement of a wavefront. RMS quantifies the magnitude of all numbers representing various height dimensions for the surface of the wave. MetroPro measures the wavefront in terms of waves, which relate the physical dimension of displacement as a ratio of the frequency of the measurement wavelength. The wavelength used is 632.8nm. Comparison of RMS values is the primary means to compare results for this thesis.

D. MASKING

A mask was applied to the interferometer as the device only measures a circular aperture, but the DM used was square. The mask prevented measurements occurring outside the area of interest. The image in Figure 16 shows the interferometer readout of the 492-SLM DM on the MetroPro software before masking was applied, Figure 16 (a), and after masking was applied, Figure 16 (b), before segments were actuated.

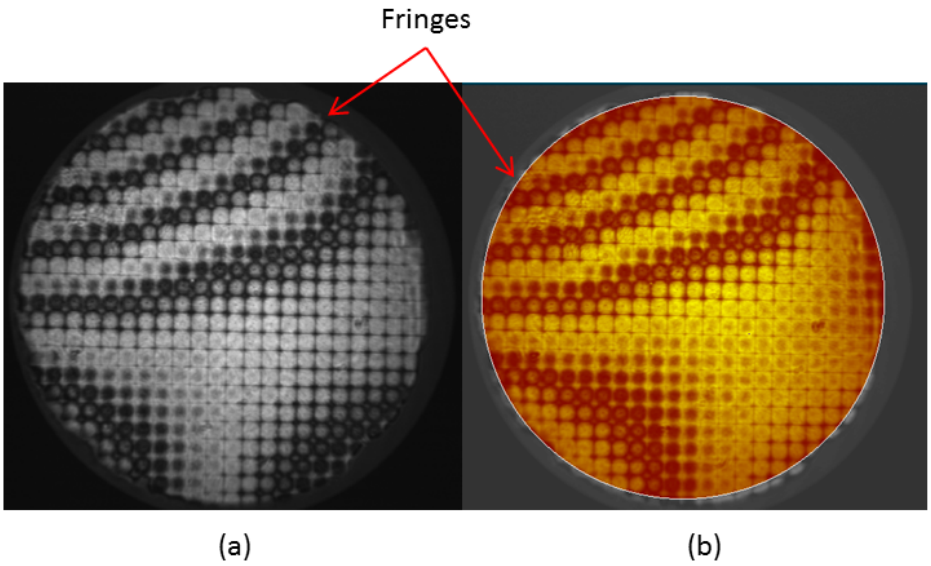

Live interferometric reading before application of the mask (a) and after (b). The mask blocks out regions so that they are not measured. Only the area in (b) shaded in red will be measured by the MetroPro software. The stripes appearing on the image are fringes, which are indications of how in focus the image is.

Figure 16. Interferometric Raw Image Before (a) and After (b) Masking

The individual segments of the DM are clearly seen in Figure 16 due to the high resolution of the interferometer. The light circular ring between the DM at the center and the darker square region encompassing the DM is the total area measured by the interferometer in Figure 16(a). A mask, as shown by the dark red circle in Figure 16 (b), was applied so that the area in red would be measured and displayed on the MetroPro software. The alternating light and dark spots are interference fringes caused by the beam of light being out of phase. Each subsequent fringe is one wavelength out of phase from its predecessor.

E. INFLUENCE MATRIX

The influence function represents the response of the mirror surface due to the actuation of a single actuator. The collective group of influence functions for each actuator is known as the influence matrix and is the total response of the surface of the DM due to actuation. For this experiment, the functions were calculated by taking an initial reference flat reading by applying 50V to all actuators and storing the resulting

wave front error in MetroPro. Then, each actuator was applied with an additional 50V and the subsequent error reading was recorded. In between each individual actuation, a reference flat measurement was obtained. For each actuator, the mean of the difference between the actuated function and the reference flat image was subtracted from the associated reference function to create the influence function for that actuator. This process was repeated to create the influence matrix. An example of an initial flat reading is shown in Figure 17.

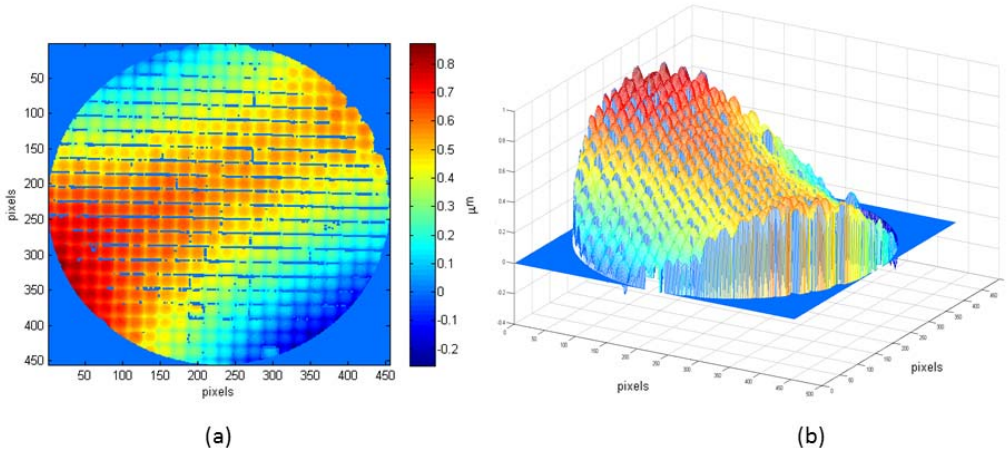

2D (a) and 3D (b) reference flat images for the Boston 492-SLM DM. For this condition, all actuators had 50V applied in order to pull the actuators to a reference plane as shown in order to establish a baseline. Red indicates high points while blue low points.

Figure 17. 2D (a) and 3D (b) Boston 492 Reference Flat Images

From Figure 17 it can be seen that even though all actuators had the same voltage applied they did not all pull down the same distance. The effects of astigmatism are seen in the saddle shape of Figure 17 (b) and tilt in Figure 17 (a) from the dark blue in the negative direction extending to the ridge in the image. Aberrations for the flat reference varied from each image. For this particular reference, a variation of approximately $1\mu m$ was measured across the surface of the mirror. This variation is significant as the segmented DM only has a stroke of $3.5\,\mu m$. This means that nearly one-third of the DM's stroke was used to correct for variance in the mirror vice optical aberrations. Drop out in the data can also be seen in many of the spaces between actuator segments,

particularly in Figure 17 (a) with the dark blue horizontal and vertical lines. This is a result of the interferometer's inability to take a measurement. However, the drop out in data does cause the correct dome shape for each actuator to be clearly visible in Figure 17 (b), indicating a correct linear response. The interferometric image is in agreement with Bifano et al. in Figure 9 to include the loss of data between segments.

F. ZERNIKE POLYNOMIALS

Before the aberrations can be corrected, the missing data must first be filled in to avoid discontinuities. Zernike polynomials were fitted to the measured reference flat to correct for the missing data points. Zernike polynomials are a series of polynomials orthogonal to a unit disk. A sum of Zernike polynomials is used to construct a wavefront for the measured data by matrix inversion:

$$\varphi(\rho,\theta) = \sum_{i=1}^{M} a_i Z_i(\rho,\theta), \tag{4.1}$$

where $Z_i(\rho,\theta)$ represents the fitted Zernike polynomial evaluated at (ρ,θ) on the unit disk while a_i are the Zernike coefficients. *M* is the number of Zernike polynomials fitted. For the experiment, a value of 50 was chosen. θ is the sum of the evaluated Zernike polynomials. Using this method, the data shown in Figure 17 can be reconstructed to the data in Figure 18.

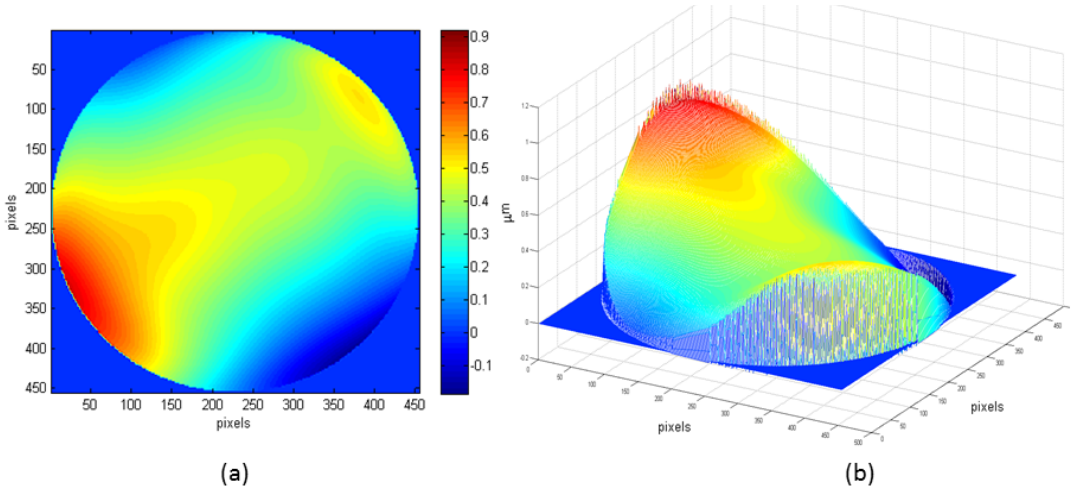

2D (a) and 3D (b) Zernike fitted reference flat images from Figure 17. Using Equation 4.1, the raw data was fitted for an *M*=50. This was done to remove discontinues. Red indicates high points while blue low points.

Figure 18. 2D (a) and 3D (b) Zernike Fitted Reference Flat

Tilt and astigmatism greatly affected the influence function as each actuator was at a slightly different initial starting height. As previously mentioned, the interferometer cannot read a difference of 2π between an actuator and its surroundings. This measurement error contributed to the variance in height of each actuator along the dimensions of the DM despite applying the same voltage to each actuator. Figure 19 shows the actuation of two different segments with the background removed. Everything except the actuator was forced to zero to remove background. This was accomplished by identifying the pixel location for each actuator and setting all areas outside of that region to zero. Figure 19 displays the difference in height for actuator 8 and 58 despite having the same voltage applied.

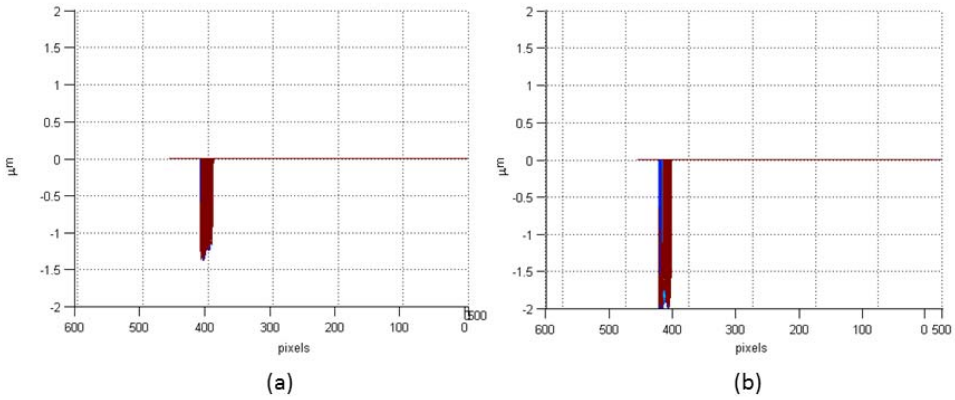

Variance in actuator piston height for actuator 8 (a) and actuator 58 (b) given the same 100 volts. An approximate 0.8 μm difference exists between these actuators despite the same identical voltages.

Figure 19. Variance in Actuator 8 (a) and Actuator 58 (b) Heights

As previously discussed, nearly one-third of the stroke for each actuator is used to correct the mirror surface vice the optical aberrations. Since this study is focused on the ability of the DM to correct for optical aberrations, piston, tip, and tilt were removed from the measured data by the MetroPro software. These aberrations would have saturated the stroke of each actuator before the DM could correct for the wavefront.

G. MIRROR CORRECTION

The surface of the Boston DM was measured after an initial 50V was applied to all actuators to make a reference flat image. The DM was then commanded to correct for an imputed distorted wavefront. A comparison of the before and after RMS values is shown in Table 1.

Table 1. Experimental Before and After RMS Values

	RMS (waves)
Before Correction	1.546
After Correction	0.883

The before correction represents the RMS reading by the MetroPro software after an initial 50V had been applied to all actuators. The after correction is the subsequent RMS value with the DM actively trying to deform its surface in order to reduce the RMS value.

The DM was able to reduce the RMS of the original distorted wavefront by approximately 54.9% (Table 1). While the corrected wavefront is not perfectly flat, the results indicate that a DM has the potential to increase optical performance.

IV. EXPERIMENTAL VERSUS MODEL RESULTS

A. MODEL SIMULATION RESULTS

A random sinusoidal wavefront was generated in order to represent the initial reference image for which the DM models were to correct (Figure 20). This is similar to the previous reading taken in the experimental lab data with the exception that the wave generated has a smooth distortion.

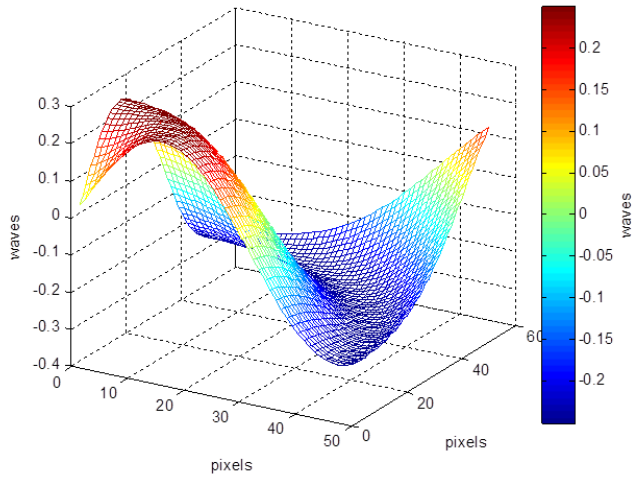

Randomly generated sinusoidal wavefront substituted into the control as the aberration coming off of a mirror for the MATLAB-generated segmented DM model to correct for.

Figure 20. Generated Wavefront Aberration for Model Testing

The wave shown in Figure 20 did not need Zernike polynomials fitted to it because it did not have any discontinuities when produced by MATLAB. A square 36 actuator segmented DM was built using the model previously constructed in Chapter II. This segmented DM model then attempted to correct for the wavefront seen in Figure 20 in order to make the wave as flat as possible. Figure 21 is a comparison of the wavefront before and after correction by the modeled segmented DM.

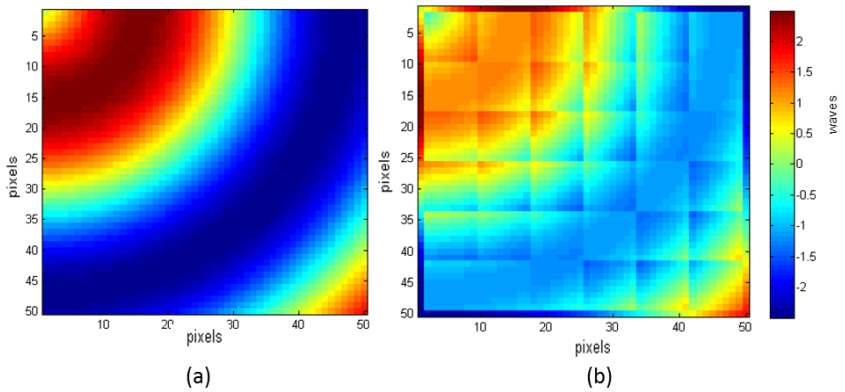

The wavefront before correction (a) has a sinusoidal pattern with red indicating a high elevation and blue as a low elevation. After correction by the 36 segmented DM (b) model the deviation behind red and blue is significantly reduced.

Figure 21. Before (a) and After (b) Comparison of Wavefront with the Segmented DM Model

The image in Figure 21(b) is not perfectly flat; a flat image would appear monochromatic. The peak of the wave can be observed in the upper left hand corner of Figure 21(b) along with the dark blue band crossing the middle, however, the difference in wave height is reduced between the before and after wave. This difference is seen in the lighter intensity of the colors as seen in Figure 21 (b), which indicates the values are closer to zero. A perfectly monochromic image is difficult to achieve in practical applications; if the error is less than one-fourteenth of a wave, the system is considered to be nearly perfect [15]. Therefore, comparison of the before and after RMS values is the best indication of performance. Figure 21 (a) has an RMS value of 0.2921 waves while after correction by the DM, as shown in Figure 21 (b), has an RMS of 0.0969 waves. This is an improvement of 100.4% in reduction of the wavefront error by the segmented DM. The corrected value is still slightly above near perfect conditions of 0.07 waves.

A segmented DM suffers from gaps between actuator pieces, which prevents the wavefront from correction at this location. These gaps are collectively represented as the uncorrected border seen in Figure 21 (b), which appears between both x and y axis locations and the start of the DM segments. As they cannot reflect light, these gaps also reduce the number of photons reaching the focal plane. This reduces the intensity, which necessitates a longer integration time at the focal plane to produce the image while

making up for the lower number of photos. The original wave undergoing correction had a smooth wavefront. However, the segmented DM was trying to fit a square/linear shape to the smooth appearance; this resulted in a staircase appearance in the corrected wavefront. The simulation can be improved by increasing the number of actuators over the same horizontal and vertical dimensions. This would enable each actuator segment to influence a smaller surface area of the wavefront. The smaller influence per actuator results in finer precision by minimizing the step distance between adjacent actuators correcting for differences in height.

Similarly, a 36-actuator continuous face sheet DM was also modeled and given the same wavefront as shown in Figure 20. The continuous DM attempted to minimize the surface error, as shown in Figure 22. The dimensions for the continuous wavefront are slightly reduced compared to the segmented DM, as a result of no gap between segments.

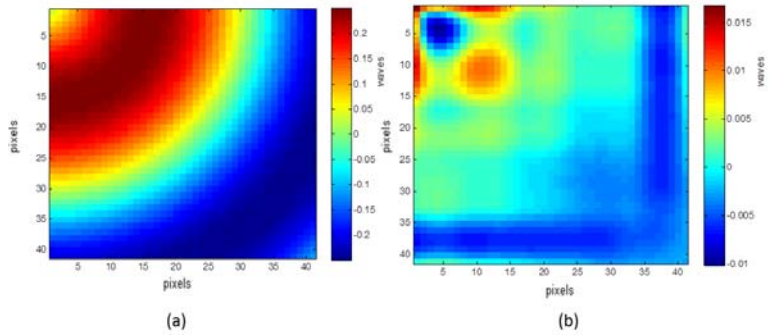

The wavefront after utilizing a square 36 continuous DM to correct for the wavefront from Figure 20.

Figure 22. Before (a) and After (b) Comparison of Wavefront with the Continuous DM Model

The continuous DM was more successful in flattening the wavefront as compared to the segmented results, but the results were still not monochromatic. Increased performance in reduction of the wavefront is confirmed in the comparison of the RMS values. Before correction, the wave had an RMS of 0.2819 waves and after a value of 0.0064 waves. This is an improvement of 191.1% and is within the near perfect threshold of 0.07 waves.

The continuous DM does not have gaps between actuators. This allows the DM to correct for the entire surface of the wavefront. Additionally, the continuous DM is trying to fit its curved surface to that of the original bowed and smooth face of the original wave. This enables the DM to achieve a closer fit as it is applying a polynomial fit as opposed to a linear fit. The absence of a gap between actuators is also attractive as it enables a shorter integration time on the focal plane due to the greater number of photons collected as compared to the segmented DM. Again, increasing the actuator density over the same area has the potential to show increased performance. However, a drawback of the continuous DM is the longer computational time. While speed is a function of the specific computer used, the ratio of computational time was approximately 2 to 1 with the continuous DM taking twice as long as that of the segmented DM to arrive at a solution. For laboratory work, this difference is irrelevant, but for practical applications it would require a continuous DM system to possess greater computational power, which increases hardware, weight, power, complexity, and cost constraints for timely application over a segmented system. The already low initial power and weight footprint of these devices makes any additional gains marginal drawbacks.

The results two DM models are compared in Table 2. The small difference in the starting RMS value is a result of the segmented DM having a slightly larger pixel area due to the spacing between actuator segments. However, despite the minor difference in the before value, the after correction value is an order of magnitude different in favor of the continuous DM. This indicates that continuous DM is preferential to a segmented DM for wavefront correction.

Table 2. Simulation Results for Before and After RMS Correction

	RMS (waves)	
	Segmented DM	Continuous DM
Before Correction	0.2921	0.2819
After Correction	0.0969	0.0064

Comparison of RMS values for the segmented and continuous DM model results utilizing a 36 actuator DM to correct for a smooth sinusoidal wavefront.

The continuous DM performed 175% better than the segmented DM for the two simulations when comparing the after RMS values. For this simulation, the continuous DM was the only one that exceeded the acceptable near-perfect RMS condition, suggesting that the continuous model is the recommended device to use for further research. Similarly to the results given in Table 1, both DM models were able to improve the wavefront, but were unable to flatten the reconstructed wavefront entirely (Table 2). To increase performance in addition to actuator density, the stroke of each actuator could be increased to give each actuator a larger dynamic range. In the MATLAB model results, stroke was not a factor given the low initial starting RMS value before correction. However, stroke likely did play a part in the results shown in Table 1 due to the greater initial RMS value of the mirror. This could have saturated the piston motion of the DM, preventing it from correcting the wavefront in either the full up or down direction beyond the saturation limit.

B. MODEL USER APPLICABILITY

MEMS deformable mirrors can provide a multitude of benefits to the U.S. Navy and Department of Defense (DOD) in general. The ability to control and shape the wavefront is ideal for laser applications. Atmospheric distortions, thermals, and differences in environments between the laser destination and target can result in laser beam distortion. These environmental factors could negate the effect of the laser by the time it reaches its destination. A DM would allow the laser to shape the wavefront at the origin such that after passing through the environment it would arrive at the target in the correct wavefront form. Instead of working against the environment or trying to burn through it simply by increasing power, DMs would enable the system to work with the environment to achieve the desired effect. In particular, a MEMS mirror plays a crucial role due to its compact size and low power consumption, making it ideal for use inside of an aerial platform or other volume-constrained products. These restricted applications include fiber optic cables for long distance data transfer and fast tactical communications such as long-distance laser communication systems.

These types of devices are also ideal for space-based applications. Space vehicles are inherently power, weight, and volume limited. This is particularly true for remote sensing systems, which require optics of superior quality that are not only heavy, but also cost prohibitive. A MEMS DM is a means to allow lighter materials with some optical aberrations on their surface to be used as mirrors in the telescope. A DM could be used to correct for the reduced optical quality of the lighter materials. In addition to surface errors, the DM could also correct for field angle magnification effects. These effects are a result of the difference in diameter of the primary mirror and that of the exit pupil. Further errors are introduced to the system as the field of view is steered across the field of regard. This causes light to enter the telescope at different angles, resulting in varying path lengths for the rays by the time the light reaches the focal plane. The DM also has potential to correct for this difference in the optical path.

V. CONCLUSION AND FUTURE WORK

This thesis successfully constructed models for both a segmented and continuous DM. Surface maps from the model were experimentally compared to measured surface maps, indicating that the models were in agreement. Experimental results using a segmented DM conducted in a laboratory environment compared well with results from the model in partially correcting a wavefront, but were unable to correct a wavefront completely.

Modeling revealed that while the continuous DM was computationally intensive, it yielded the most success in reducing the wavefront. For the simulation, the continuous model reduced the before and after RMS value by a factor of 191% while the segmented DM only improved RMS by 100% despite using the same number of actuators. This difference can be contributed to the fact that the segmented DM is limited to correcting in a linear fashion while the continuous DM can flex its surface along a curved path creating a polynomial fit to the surface. Additionally, the segmented DM must contend with gaps between actuator segments, which not only results in a loss of photons, but also restricts wavefront correction at these locations. Gaps between segments in relation to the wavefront leave this portion of the wave uncorrected. The continuous DM is also able to phase, which allowed it to achieve a closer fit to the originally smooth distortion while the segmented DM assumed a step like appearance. In the simulation, the segmented DM achieved a corrected wavefront value of 0.0969 waves while the continuous DM had a wavefront error of 0.0064 waves, below the threshold of near perfect of 0.07 waves.

A number of factors could be adjusted to improve performance. The number of actuators for a given wavefront can be increased in addition to the stroke of each actuator. The DMs could also be combined such that the wavefront is corrected in series. In such a scenario, an initial DM would provide course correction and additional DMs could fine tune control of the wavefront. The continuous DM is the most likely candidate for this due to its better ability to correct for the wavefront and the fact that it does not lose photons between actuator segments because of gaps.

A. SUITABILITY OF MEMS IN THE SPACE ENVIRONMENT

MEMS deformable mirrors have immense potential for space-based telescopes for the DOD and Intelligence Community. Current remote sensing satellites use large and expensive primary mirrors that are of exceptional optical quality. Weight and cost savings could be achieved by using cheaper and/or lighter material at the expense of reduced optical quality. Placing a DM in the optical path of a telescope could help overcome the optical defects of the new material by correction for these aberrations.

For space-based applications, the DM would not only have to contend with the wavefront itself, but also magnification factors due to field angles. The field angles from these systems having a wide field of view in which a fast steering mirror typically navigates the field of view across the field of regard of the telescope. This results in light striking the focal plane array at different angles. A magnification factor results from the difference in diameter of the primary mirror and that of the width of the light ray at the exit pupil location. To be effective, a DM would need to resolve these factors. A notional telescope could be designed that places a DM at the exit pupil location that attempts to correct for a hypothetical wavefront while contending with the additional factors.

B. CONTINUOUS FACE SHEET MEMS DEVICE

A segmented DM was used for the experimental test setup. However, the models showed that a continuous DM offers far greater potential in its ability to reduce the RMS. Laboratory experiments could be conducted using a continuous DM given the same wave front in the lab to observe the correction ratios of RMS values in the lab compared to the correction ratio for the models.

Additionally, the number of actuators and length of stroke for each actuator could be adjusted in order to characterize how parameters affect performance. This could be related to the wavelength of interest to determine if there is a limit at which increasing the actuator count or stroke no longer improves performance.

A group of continuous DMs can be placed in a series such that instead of one mirror trying to correct for an entire wavefront, a series of mirrors could be used to correct different aspects of the wavefront. Results from this series of DMs could be

compared with the results of simply having one DM with more actuators and increased stroke. Both simulations and laboratory experiments could be conducted to more accurately correct for distortions.

This ability to fine tune control of the wavefront could be of value to laser propagation. This is particularly important in a maritime environment where the atmosphere above the sea surface is consistently turbulent and has constantly changing parameters such as humidity, winds, particulates, temperature etc. A laser needs to penetrate these atmospherics to be effective in reaching a target at an appreciable distance. A DM can facilitate fine-tuned control of the laser so that it could adapt the wavefront as necessary to the atmospherics of its environment.

THIS PAGE INTENTIONALLY LEFT BLANK

APPENDIX. MATLAB CODE

A. CONTINUOUS MEMS MIRROR MODEL MATLAB CODE

```
a=455;   %  mirror length
b=455;   %  mirror width

R=100;  %Number of actuators
rows=sqrt(R);
colomns=rows;

gi = 2;    % Gaussian Index: Usually from 1.5 to 2.5

for j=1:R
Vc=zeros(R,1);
Vc(j)=-1;

%Actuator spacing
x=a/rows:a/rows:a;
x=repmat(x,1,rows);
y=x;

%Calculates the wave
for i=1:R
    for xx=1:length(x)
        for yy=1:length(y)
            wave(i)=Vc(i)*(2*pi)*exp(log(gi)*(x(i)^2+y(i)^2)/(a/R)^2);
            %wave(i)=(1-3.*xx(i).^2+2.*xx(i).^3).*(1-
3.*yy(i).^2+2.*yy(i).^3); %Tyson Page 187 Eqn 6.13
        end
    end
end

%Imposes stroke limitation
for i = 1 : R
    if wave(i) < -1.5e-6; % Anything less than this value will be set
to zero
        wave(i) = -1.5e-6;;%-1.5e-6;
    end
end
wave(isnan(wave))=0;

w=reshape(wave,rows,colomns);
w=interpn(w,'cubic');
w=interpn(w,'cubic');
w=interpn(w,'cubic')/1e-6;

IF(:,j)=reshape(w',[numel(w) 1]);


%For graphing
```

```
count=1;
for i=1:length(w)
    for xx=0:length(w)-1
        x(count)=a/(2*length(w))+(a/(2*length(w)))*xx*2;
        count=count+1;
    end
end
y=x;
x=x(1:length(w));
y=y(1:length(w));

%Graphs
F(R) = struct('cdata',[],'colormap',[]);
figure(1)
figureTitle1 = sprintf(' 3D View Actuator #%01d Influence',j);
subplot(2,4,[1 2 5 6]), mesh(x,y,w);
%subplot(2,4,[1 2 5 6]); sp=spaps({x,y},w,0); fnplt(sp)
%subplot(2,4,[1 2 5 6]); sp=surf(x,y,w); shading interp
title(figureTitle1);
xlabel('pixels');
ylabel('pixels');
zlabel('\mu m')
wmin=floor(min(w(:)));
wmax=ceil(max(w(:)));
winc=(wmax-wmin)/60;
wlevs=wmin:winc:wmax;
subplot(2,4,[3 4 7 8]), imagesc(x,y,w); %colormap gray
h=colorbar;
ylabel(h, '\mu m')
figureTitle2 = sprintf(' Top View Actuator #%01d Influence',j);
title(figureTitle2);
xlabel('pixels');
ylabel('pixels');

figure(2)
imagesc(x,y,w); %colormap gray
h = colorbar;
ylabel(h, '\mu m')
figureTitle2 = sprintf(' Top View Actuator #%01d Influence',j);
title(figureTitle2);
xlabel('pixels');
ylabel('pixels');

F(i) = getframe;
pause()
end
```

B. SEGMENTED MEMS MIRROR MODEL MATLAB CODE

```
a=455;   %  mirror length
b=455;   %  mirror width

R=100;  %Number of actuators
```

```
rows=sqrt(R);
colomns=rows;

gi = 2;    % Gaussian Index: Usually from 1.5 to 2.5

for j=1:R
Vc=zeros(R,1);
Vc(j)=-1;

%Actuator spacing
x=a/rows:a/rows:a;
x=repmat(x,1,rows);
y=x;

%Calculates the wave
for i=1:R
    for xx=1:length(x)
        for yy=1:length(y)
            wave(i)=Vc(i)*(2*pi)*exp(log(gi)*(x(i)^2+y(i)^2)/(a/R)^2);
            %wave(i)=(1-3.*xx(i).^2+2.*xx(i).^3).*(1-
3.*yy(i).^2+2.*yy(i).^3); %Tyson Page 187 Eqn 6.13
        end
    end
end

%Imposes stroke limitation
for i = 1 : R
    if wave(i) < -2e-6 % Anything less than this value will be set to
zero
        wave(i) = -2e-6;
    end
end

%Segments (Must match the controls script)
phi=zeros(50);
x=linspace(0,1,50);
y=x;
[x_grid,y_grid] = meshgrid(x,y);

count=j;
if wave(j)<0
    colomnlocation=round(ceil(count/rows));
    subfactor=floor((count/rows)-0.01);
    rowlocation=round(((count/rows)-subfactor)/(1/rows));

    phi(find(x_grid>(colomnlocation-1)/rows & x_grid <
colomnlocation/rows & y_grid >(rowlocation-1)/rows & y_grid <
rowlocation/rows))=wave(j);
    count=count+1;
end

IF(:,j)=reshape(phi',[numel(phi) 1]);
```

```
%Graphs
F(R) = struct('cdata',[],'colormap',[]);
figure(1)
figureTitle1 = sprintf(' 3D View Actuator #%01d Influence',j);
subplot(2,4,[1 2 5 6]), mesh(x_grid*a,y_grid*b,phi);
%subplot(2,4,[1 2 5 6]); sp=spaps({x,y},w,0); fnplt(sp)
%subplot(2,4,[1 2 5 6]); sp=surf(x,y,w); shading interp
title(figureTitle1);
xlabel('\mu m');
ylabel('\mu m');
zlabel('\mu m');
subplot(2,4,[3 4 7 8]), contour(x_grid*a,y_grid*b,phi); colormap jet
figureTitle2 = sprintf(' Top View Actuator #%01d Influence',j);
title(figureTitle2);
%colorbar('location','southoutside')
xlabel('\mu m');
ylabel('\mu m');

figure(2)
contour(x_grid*a,y_grid*b,phi); colormap gray
h = colorbar;
ylabel(h, 'nm')
figureTitle2 = sprintf(' Top View Actuator #%01d Influence',j);
title(figureTitle2);
xlabel('pixels');
ylabel('pixels');

F(i) = getframe;
pause()

end
```

LIST OF REFERENCES

[1] K.M. Morzinksi, J. W. Evans, S. Severson, B. Macintosh, D. Dillon, D. Gavel, C. Max, and D. Palmer, "Characterizing the potential of MEMS deformable mirrors for astronomical adaptive optics," *Proc. SPIE*, 2006, vol. 6272, 77362D.

[2] J. B. Steward, A. Doiuf, Y. Zhou, and T. G. Bifano, "Open-loop control of a MEMS deformable mirror for large amplitude wavefront control," *J. Opt. Soc. Am. A2007,* vol. 24, is. 2, pp. 3827–3883.

[3] J. Stewart, T. Bifano, S. Cornelissen, P. Bierden, B. Levine, and T. Cook "Design and development of a 329 segment tip-tilt-piston mirror array for space-based adaptive optics," SPIE, 2006, vol. 6113, 61130O.

[4] A. Papvasiliou, S. Olivier, T. Barbee, C. Walton, and M. Cohn, "MEMS actuated deformable mirror," *Proc. SPIE*, 2006, vol. 6113, pp. 190–199.

[5] O. A. Azucena, B. F. Fernandex, and J. A. Kubby, "Nonlinear plate equation analysis for the design of large stroke deformable mirror," *Proc. SPIE*, 2008, vol. 6888, 68880Q.

[6] S. Timoshenko and S. Woinowsky-Krieger, *Theory of Plates and Shells*. New York: McGraw-Hill Publishing, 1976.

[7] R. Szilard, *Theory and Analysis of Plates: Classical and Numerical Methods.* Upper Saddle River, NJ: Prentice Hall Publishing, 1974.

[8] B. Johnson and D. V. Murphy. "Thermal blooming laboratory experiment, Part I. In *Lincoln Laboratory MIT Project Report*, Cambridge, MA: MIT Press, 1988.

[9] H. Xing Yan, S. Li, D. Zhang, and S. Chen: "Numerical simulation of an adaptive optics system with laser propagation in the atmosphere," *Applied OPTICS*, 2000, vol. 39, is 18, pp. 3023–3031.

[10] A. Helmbrecht, T. Juneau "Piston-tip-tilt positioning of a segmented MEMS deformable mirror," *Proc.* SPIE, 2007 vol. 6467, 64670M.

[11] R. Hudgin, "Wavefront compensation error due to finite corrector-element size," *J. Opt. Soc. Am.* 1977, vol. 67, is. 3, pp. 393–395.

[12] R. K. Tyson, *Principles of Adaptive Optics*, 3rd ed. Boca Raton: Academic Press, 1998.

[13] T. Bifano, J. Perreault, R. Mali, M. Horenstein "Mircroelectromechanical Deformable Mirrors," in *IEEE Journal of Selected Topics in Quantum Electronics,*1999, vol. 5, no. 1, pp.83–89.

[14] E. Villalba, “Reducing the surface performance requirements of a primary mirror by adding a deformable mirror in its optical path,” M.S. thesis, Space Sys. Dept., Naval Postgraduate School, Monterey, CA 2015.

[15] P. Bely, *Design and Construction of Large Optical Telescopes*. New York, NY: Springer-Verlag Publishing, 2003.

INITIAL DISTRIBUTION LIST

1. Defense Technical Information Center
   Ft. Belvoir, Virginia

2. Dudley Knox Library
   Naval Postgraduate School
   Monterey, California